ORIGINAL ARTICLE
Polish Journal of Microbiology
2026, Vol. 75, No 1, 055-074
https://doi.org/10.33073/pjm-2026-007

Comparative Analysis of Rhizosphere Bacteria of *Phragmites australis* and *Suaeda salsa* (L.) *Pall.* on Chenier Islands

BO ZHOU[1,2], JUNPENG LIU[1,2], LINQI LI[1,2], JINGYI YU[1,2], XINGGUO SUN[3], JUN WANG[1*] and SHUAI SHANG[1*]

[1]College of Biological and Pharmaceutical Engineering, Shandong University of Aeronautics, Binzhou, Shandong, China
[2]Shandong Key Laboratory of Eco-Environmental Science for the Yellow River Delta, Shandong University of Aeronautics, Binzhou, Shandong, China
[3]Dongying Airport Company Limited, Shandong Airport Management Group, Dongying, Shandong, China

Submitted 8 September 2025, accepted 29 December 2025, published online 31 March 2026

Abstract

The Chenier Islands are depositional areas within intertidal zones, characterized by unique soil textures and distinctive environmental conditions that shape specific vegetation distribution patterns. However, the adaptive mechanisms of *Phragmites australis* (common reed) and *Suaeda salsa* (L.) *Pall.* (common seepweed) two prevalent plant species in this region—in saline stress environments, as well as the composition and functional characteristics of their rhizosphere bacterial communities, remain largely unclear. In this study, rhizosphere soil samples were collected from common reed and common seepweed. DNA was extracted and subjected to high-throughput sequencing to analyze the composition and predictive functional profiles of the rhizosphere microbial communities. The results indicated that no significant differences were observed in the alpha diversity indices (Chao1, ACE, Simpson, and Shannon), indicating similar microbial species richness and evenness in the rhizospheres of common reed and common seepweed. Taxonomic analysis at the phylum level showed that the dominant bacterial phyla shared by both plants were *Proteobacteria*, *Bacteroidota*, *Chloroflexota*, and *Actinomycetota*. Notably, *Acidobacteriota* and *Cyanobacteria* were uniquely enriched in the common reed and common seepweed rhizospheres, respectively. At the genus level, the microbial communities of both plants were largely composed of unclassified taxa and minor groups, with *Zeaxanthinibacter* being the only cultivable dominant genus identified. Principal Coordinates Analysis (PCoA) explained 75.02% of the total β-diversity variance, and the clear separation of samples along the first coordinate axis revealed visually distinct community structures between the two plants. PERMANOVA further confirmed that plant species significantly influenced microbial community assembly, with a moderate explanatory strength ($R^2 = 0.205$, $p = 0.008$). Integrated results from LEfSe, PICRUSt2, and FAPROTAX analyses demonstrated that common seepweed rhizospheres were enriched with 19 photosynthesis-related biomarkers, suggesting a stronger photoautotrophic potential compared to common reed. In contrast, the common reed rhizosphere retained only two oligotrophic degraders *Acidobacteriota* and *Chloroflexota*. Although PICRUSt2 predictions indicated high overlap in core metabolic pathways between the two plants, FAPROTAX profiling revealed markedly divergent energy-acquisition strategies. Specifically, the common seepweed microbiome exhibited a "photoautotrophy nitrogen fixation" coupling strategy, whereas common reed relied predominantly on a "chemoheterotrophy nitrate reduction" pathway, reflecting niche partitioning in the saline environment. It should be noted that functional predictions derived from PICRUSt2 and FAPROTAX are computational inferences rather than empirical measurements, and thus mechanistic interpretations should be treated with caution. This study identifies a rhizosphere bacterial community assembly pattern characterized by "structural differentiation but functional convergence" offering valuable insights into microbial-mediated plant adaptation to saline stress.

Keywords: *Phragmites australis*, *Suaeda salsa* (L.) *Pall.*, rhizosphere bacteria, functional redundancy, adaptation to saline stress

* Corresponding authors: S. Shang, College of Biological and Pharmaceutical Engineering, Shandong University of Aeronautics, Binzhou, Shandong, China; **email: shangshuai8983@126.com**
J. Wang, College of Biological and Pharmaceutical Engineering, Shandong University of Aeronautics, Binzhou, Shandong, China; **email: ivywangjun@163.com**

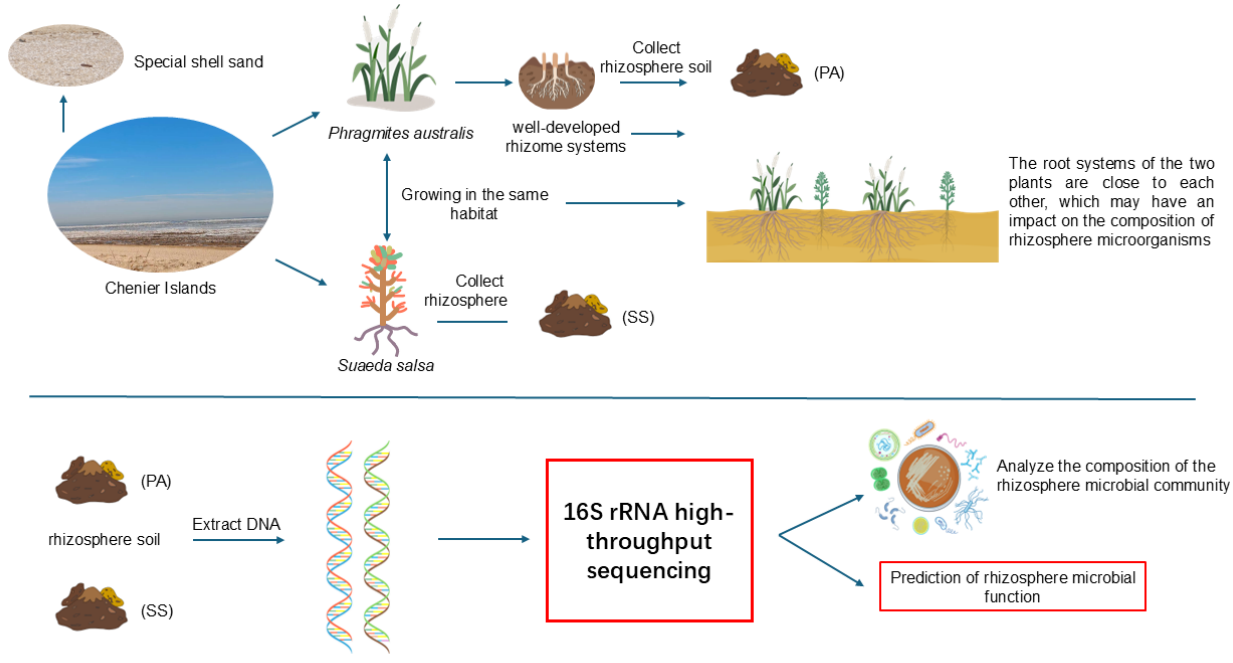

Introduction

Against the backdrop of global climate change and sea-level rise, coastal ecosystems are confronting multifaceted threats, including exacerbated salinization, biodiversity erosion, and ecological functional degradation (Tully et al. 2019). Coastal salinization, as a pervasive environmental issue, not only directly constrains coastal agriculture and ecological security but also profoundly restructures soil physicochemical properties and vegetation distribution patterns. These changes, in turn, significantly alter carbon and nitrogen cycling processes and undermine the stability of coastal wetland ecosystems (Li et al. 2024). Chenier Islands, representative tidal depositional landforms, provide a vivid record of coastline dynamics shaped by land-sea interactions. (Liu et al. 2016). These unique geomorphological features not only chronicle historical sea-level fluctuations and sedimentary dynamics but also serve as a natural laboratory for investigating coastal salinization ecological processes and plant adaptation mechanisms in the context of contemporary global change.

Chenier Islands, a globally rare intertidal depositional landform, are mainly found along the silt-muddy coasts surrounding the Bohai Sea. These islands represent a unique coastal dune formation shaped by the combined effects of tidal dynamics and the accumulation of mollusk shell debris. The soil matrix primarily consists of shell fragments intermixed with yellowish-brown fine sand (Xia et al. 2015). The distinct layered structure of shell and sand provides significant geomorphological insights into coastal ecosystems. As sensitive ecological interfaces within the land-sea transition zone, Chenier ridges serve dual functions: acting as natural barriers against storm surges and supporting specialized saline habitats and soil conditions that promote distinct vegetation patterns (Liu et al. 2005). Perennial plant species include *P. australis* and *Glycine soja* Sieb. et Zucc (wild soybean), *Limonium bicolor* (Bag.) Kuntze (seashore statice), and *Tamarix chinensis Lour*. (Chinese tamarisk), predominantly occupy key ecological niches in this region (Zhao et al. 2022), while annual halophytes, such as Common seepweed and *Suaeda glauca* (Bunge) Bunge (Seaside seepweed), are commonly found across the islands; they provide a natural laboratory for studying the adaptation mechanisms of halophytes to saline-stress environments.

Common reed, a perennial grass in the Poaceae family, has a near cosmopolitan distribution. With an extensive root system and a high reproductive capacity, this species propagates through seeds, rhizomes, and stolons to establish new ramets under favorable environmental conditions (Juneau and Tarasoff 2013). Common seepweed is an annual plant in the family Amaranthaceae, genus Suaeda. It is primarily distributed across Asia and Europe, typically found in patches

within extreme environments such as saline-alkali soils, wastelands, and tidal flats. The species exhibits a strong capacity for environmental adaptation. Under various environmental stressors, it can mitigate adverse effects by adjusting its physiological and growth characteristics (Cao et al. 2022). It exhibits strong adaptability to salt stress and is commonly found growing in saline-alkali soils, often forming monospecific communities near coastal areas and lakeshores.

The rhizosphere, the narrow region of soil influenced by plant root activity, is a complex and dynamic microecological environment. This zone offers diverse ecological niches that support a wide range of bacterial communities, which play crucial roles in plant growth, nutrient absorption, and stress tolerance (Chapman et al. 2010). The rhizosphere soil environment is central to the interactions between plants and rhizosphere-inhabiting Bacteria. Within this zone, the functioning and regulation of all biological processes are primarily determined by the dynamic interplay between plant roots and associated Bacteria populations (Solomon et al. 2024). Among the microorganisms interacting with plants, bacteria and fungi have the highest proportions, and they play essential roles in promoting plant growth, nutrient uptake, and enhancing plant stress resistance (Trivedi et al. 2020) Autotrophic nitrogen-fixing bacteria promote plant growth by accelerating phosphorus cycling in the soil and the release of heavy metal ions through processes such as nitrogen fixation, phosphate solubilization, production of siderophores, secretion of IAA (indole-3-acetic acid), and organic acids (Huang et al. 2024; Kraepiel 2009) However, not all microorganisms benefit plants; some pathogenic bacteria can cause diseases and inhibit or impair plant growth. *Phytopathogens*, including *Ralstonia pseudosolanacearum*, *Fusarium oxysporum*, *Rhizoctonia solani*, and viruses such as wheat yellow mosaic virus (WYMV), can infect root, stem, and foliar tissues, causing significant plant damage (Chen et al. 2025). The proliferation of these pathogens disrupts mutualistic plant-microbe interactions, ultimately impairing ecosystem functioning (Singh et al. 2025). Plant rhizospheres harbor abundant bacterial communities inhabiting root surfaces and the surrounding soil microenvironments. Plant species identity, rhizosphere effects, sloughed root tissues, root exudates, and diverse environmental factors collectively shape the composition of these rhizosphere microbiomes (Yetgin 2023; Pantigoso et al. 2022). Employing high-throughput sequencing techniques to characterize rhizosphere soil bacterial community composition and functionality enables the elucidation and harnessing of plant-microbe interactions to promote plant growth, sustain biodiversity, and achieve species coexistence (Yuan et al. 2022). Field investigations revealed that common reed is widely distributed across the Chenier Islands, with well-developed rhizomes interweaving into an underground network. The root network of common reed is near the root systems of common seepweed. Common reed is a perennial herbaceous plant that propagates continuously via underground rhizomes, forming stable, year-to-year persistent communities that provide a long-term, continuous rhizosphere habitat for microorganisms (Čížková and Lukavská 1999; Chen et al. 2025). In contrast, common seepweed is an annual true halophyte that completes its entire life cycle from seed germination to senescence within a single growing season (Song and Wang 2015). Furthermore, their salt tolerance strategies differ fundamentally: common reed adapts to saline environments primarily through salt avoidance and secretion mechanisms (Guan et al. 2017), whereas common seepweed evolves succulent organs for salt inclusion (Song et al. 2022). Providing an opportunity to investigate the composition, characteristics, and functions of the rhizosphere bacterial communities of common reed and seepweed and their interactions. Rhizosphere bacteria regulate plant growth through their secretions, serving as signaling molecules. Plants and their rhizosphere microbiota collectively form a holobiont, whose extended genome significantly enhances the host's phenotypic plasticity and ecological adaptability under saline stress. (Olanrewaju et al. 2019; Vandenkoornhuyse et al. 2015). Although the rhizosphere microbiota of coastal saline systems has been widely explored, it remains unclear how *P. australis* and *S. salsa,* with their interlaced root systems, achieve niche separation and adaptation to the saline environment in the special soil matrix of the Chenier Islands through differentiated rhizosphere microbiota recruitment strategies. This study hypothesized that *P. australis* and *S. salsa* employ distinct recruitment strategies for their root-associated microbiota, predicting significant structural differentiation but functional convergence in their rhizosphere microbial communities. By extracting rhizosphere soil DNA and conducting 16S rRNA high-throughput sequencing, we analyzed the composition and predictive

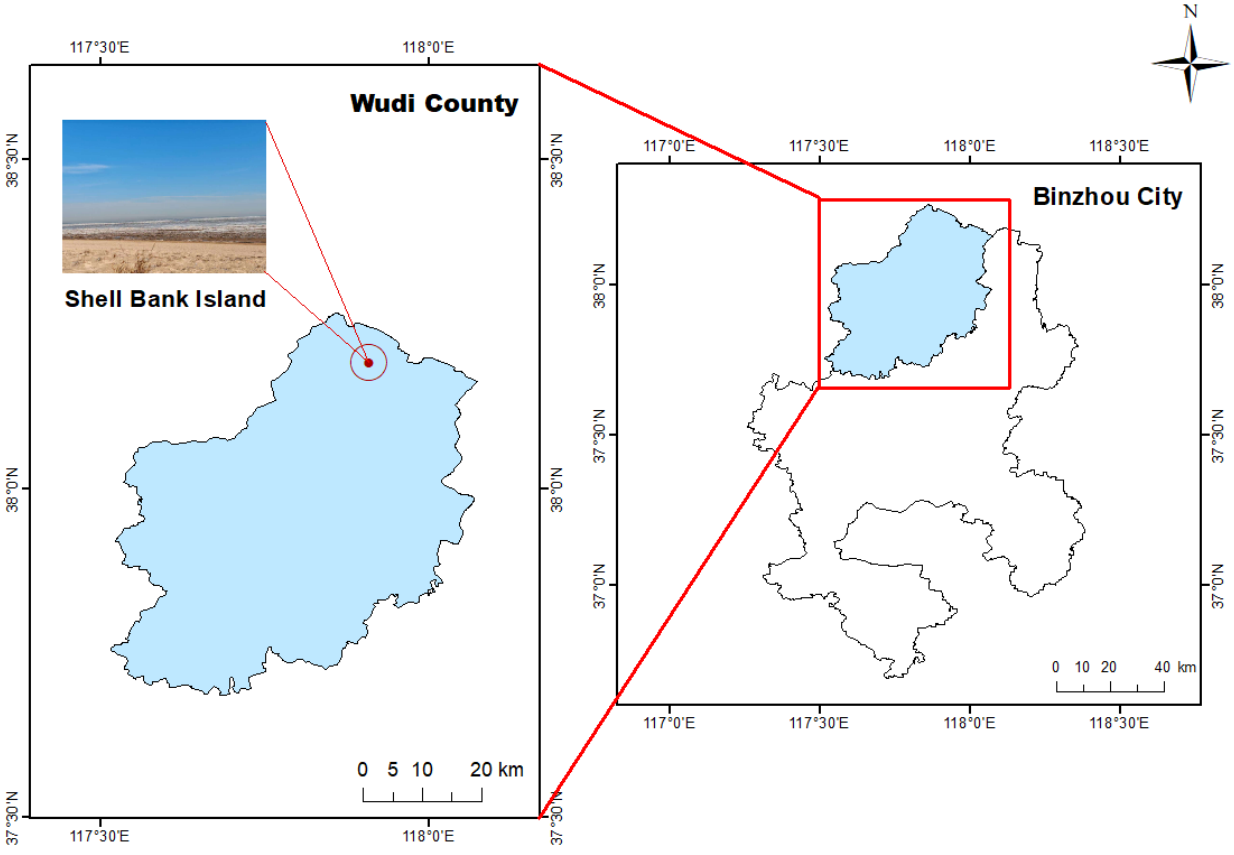

Fig. 1. Overview Map of the Study Area in the Chenier Islands.

Table I
Soil physical and chemical parameters.

Sample ID	Sample Type	EC (μs/cm)	pH
PA-1	PA	746	8.59
PA-2	PA	745	8.28
PA-3	PA	735	8.38
PA-4	PA	729	8.27
PA-5	PA	741	8.50
PA-6	PA	732	8.36
SS-1	SS	632	8.38
SS-2	SS	631	8.32
SS-3	SS	635	8.33
SS-4	SS	637	8.36
SS-5	SS	633	8.36
SS-6	SS	641	8.33

PA – *Phragmites australis* rhizosphere soil
SS – Suaeda salsa (L.) *Pall.* rhizosphere soil

functional profiles of the microbial communities associated with both plant species. This approach enabled a systematic comparison of community structure and potential functional roles, aiming to elucidate plant ecological adaptation mechanisms in the unique habitat of Chenier Islands and provide a theoretical foundation for the phytoremediation and management of coastal saline-affected areas.

Experimental

Materials and Methods

Study area and sample collection. The study area of this experiment is located within the Chenier Islands of the Yellow River Delta (37°54′30″N to 38°19′10″N, 117°45′08″E to 118°05′37″E). This region experiences a warm-temperate semi-humid continental monsoon climate, characterized by cold winters and hot summers, with four distinct seasons. The mean annual temperature ranges from 11.7°C to 12.6°C, and the average annual precipitation ranges from 530 mm to 630 mm (Zhang et al. 2021). Field sampling was conducted on April 6, 2025, in the Binzhou Shell Ridge Island and Wetland National Nature Reserve (37°54′30″ to 38°19′10″N, 117°45′08″ to 118°05′37″E). A rectangular plot of approximately 150 m × 150 m was delineated in an area where common reed (*P. australis*) and common seepweed (*S. salsa*) co-occur. Sampling points were arranged along the plot's diagonal transect, with a minimum spacing of ≥15 m between adjacent points, and avoiding areas with obvious signs of human disturbance. The plant selection criteria were

as follows: (i) absence of disease or pest symptoms; (ii) plant height within the top 25% biomass range of the plot (common reed > 30 cm, common seepweed > 15 cm); (iii) only a single individual plant collected per sampling point, with intact root systems ensured; (iv) the spatial distance between the two sampled plant species at each point not exceeding 5 m. Root systems from the 0–30 cm soil layer were carefully excavated. After gently lifting the roots and shaking off loosely adhering soil, the tightly adhering rhizosphere soil was collected by brushing the root surfaces with a sterile brush. The soil samples were then placed into sterile zip-lock bags and stored in a 4°C cooling container. A total of 12 rhizosphere soil samples (about 50 grams per sample) were obtained, comprising six biological replicates per plant species (designated as the PA group for *P. australis* and the SS group for *S. salsa*). Subsequently, impurities were removed from the samples by passing them through a sterile 2 mm sieve. Aliquots of 0.5 g to 1 g of the sieved soil were taken for DNA extraction, while the remaining soil was stored at –80°C for subsequent high-throughput sequencing of the 16S rRNA gene.

Soil physicochemical analysis. The pH and electrical conductivity (EC) of the rhizosphere soil samples were measured to assess the edaphic conditions. Air-dried soil was suspended in deionized water (1:5 w/v) and shaken for 30 minutes. The pH was determined using a digital pH meter, and EC was measured using a conductivity meter. Measurements were performed in triplicate for each sample.

High-Throughput Sequencing of soil microbes. Total genomic DNA was extracted from rhizosphere soil samples of *P. australis* and *S. salsa* using the TGuide S96 Magnetic Soil/Stool DNA Kit (Tiangen Biotech, China), following the manufacturer's protocol. The quality and integrity of the DNA were assessed by 1.8% agarose gel electrophoresis, while concentration and purity were determined using a NanoDrop 2000 spectrophotometer (Thermo Scientific, USA). The V3-V4 hypervariable region of the bacterial 16S rRNA gene was amplified using the primer pair 338F (5′-ACTCCTACGGGAGGCAGCA-3′) and 806R (5′-GGACTACHVGGGTWTCTAAT-3′) (Takahashi et al. 2014). Both forward and reverse primers were tailed with sample-specific Illumina index sequences to enable multiplexed deep sequencing. Libraries were constructed with the Illumina TruSeq Nano DNA LT Library Prep Kit (FC-121-4001). The workflow consisted of: end repair and A-tailing (50°C for 30 min, 72°C for 5 min); ligation of universal adapters (P5: 5′-AATGATACGGCGACCACCGAGAUCTACAC-3′; P7: 5′-CAAGCAGAAGACGGCATACGAGAT-3′) at a final concentration of 15 μM double-size selection with AMPure XP beads (0.8× followed by 0.2× ratios) to enrich for 300–500 bp insert fragments and a 12-cycle PCR enrichment to incorporate the 8 bp dual-indexes. The final libraries showed a primary peak of 460–480 bp and were quantified and normalized to 2 nM. The 20 μl PCR mixture comprised: 5–50 ng of DNA template, 0.3 μl each of forward and reverse primers (10 μM), 5 μl of KOD FX Neo Buffer, 2 μl of dNTPs (2 mM each), 0.2 μl (1.0 U) of KOD FX Neo DNA Polymerase (Toyobo, Japan), and ddH_2O up to 20 μl. The thermal cycling conditions were: initial denaturation at 95°C for 5 min; 20 cycles of denaturation at 95°C for 30 s, annealing at 50°C for 30 s, and extension at 72°C for 40 s; with a final extension at 72°C for 7 min. PCR amplicons were purified using the Omega DNA Clean Kit (Omega, USA), quantified on a Qsep-400 Bio-Fragment Analyzer (Bioptic, Taiwan), and subjected to paired-end (2 × 250 bp) sequencing on an Illumina NovaSeq 6000 platform (Biomarker Technologies, China).

Bioinformatic analysis. According to quality of single nucleotide, raw data was primarily filtered by Trimmomatic (Bolger et al. 2014) (version 0.33) was used with parameters SLIDINGWINDOW:4:20 MINLEN:200 (4-base sliding window with average quality ≥ Q20, reads shorter than 200 bp were discarded) Adapter removal criteria: Cutadapt v1.9.1 was used to identify and remove primer sequences, allowing ≤ 2 mismatches at the 3′ end. After filtering, an average of 69,498 high-quality reads was retained per sample, with a minimum of 53,136 high-quality reads retained per sample. Identification and removal of primer sequences was performed by Cutadapt (Martin 2011) (version 1.9.1). PE reads obtained from previous steps were assembled by USEARCH (Edgar 2013) (version 10) and followed by chimera removal using UCHIME (Edgar et al. 2011) (version 8.1). The high-quality reads generated from the above steps were used for subsequent analyses. Clean reads were then subjected to feature classification via DADA2 trunc-len-f 240, max-ee 2) (Callahan et al. 2016) to generate amplicon sequence variants (ASVs). This method identifies exact sequence variants without relying on sequence similarity clustering. ASVs with counts < 2 across all samples were filtered out. Taxonomic annotation of ASVs was performed using the Naive Bayes classifier in QIIME2 (Bolyen et al. 2019) against the SILVA database (Quast et al. 2012) (release 138.1) with a confidence threshold of 70%.

Statistical analysis. The DADA2 (Callahan et al. 2016) method in QIIME2 2020.6 (Bolyen et al. 2019) was employed to denoise, merge paired-end sequences, and remove chimeric sequences, yielding the final valid data. Following ASV table generation, Venn diagrams were constructed to visualize ASV overlap among samples, and shared microbial features across environments were identified based on taxonomic annotation. Taxonomic annotation of feature sequences was performed using a Naive Bayes classifier trained on the SILVA reference database. Following taxonomic annotation, ASVs assigned to chloroplasts (taxonomic label: p__Chloroplast) and mitochondria (taxonomic label: p__Mitochondria) were removed using the QIIME2 feature-table filter-taxa command to eliminate plant organelle contamination. Species distribution bar plots across taxonomic levels were generated using QIIME software. Alpha diversity indices (ACE, Chao1, Simpson, Shannon) were calculated in QIIME2. Statistical differences between groups were assessed us-

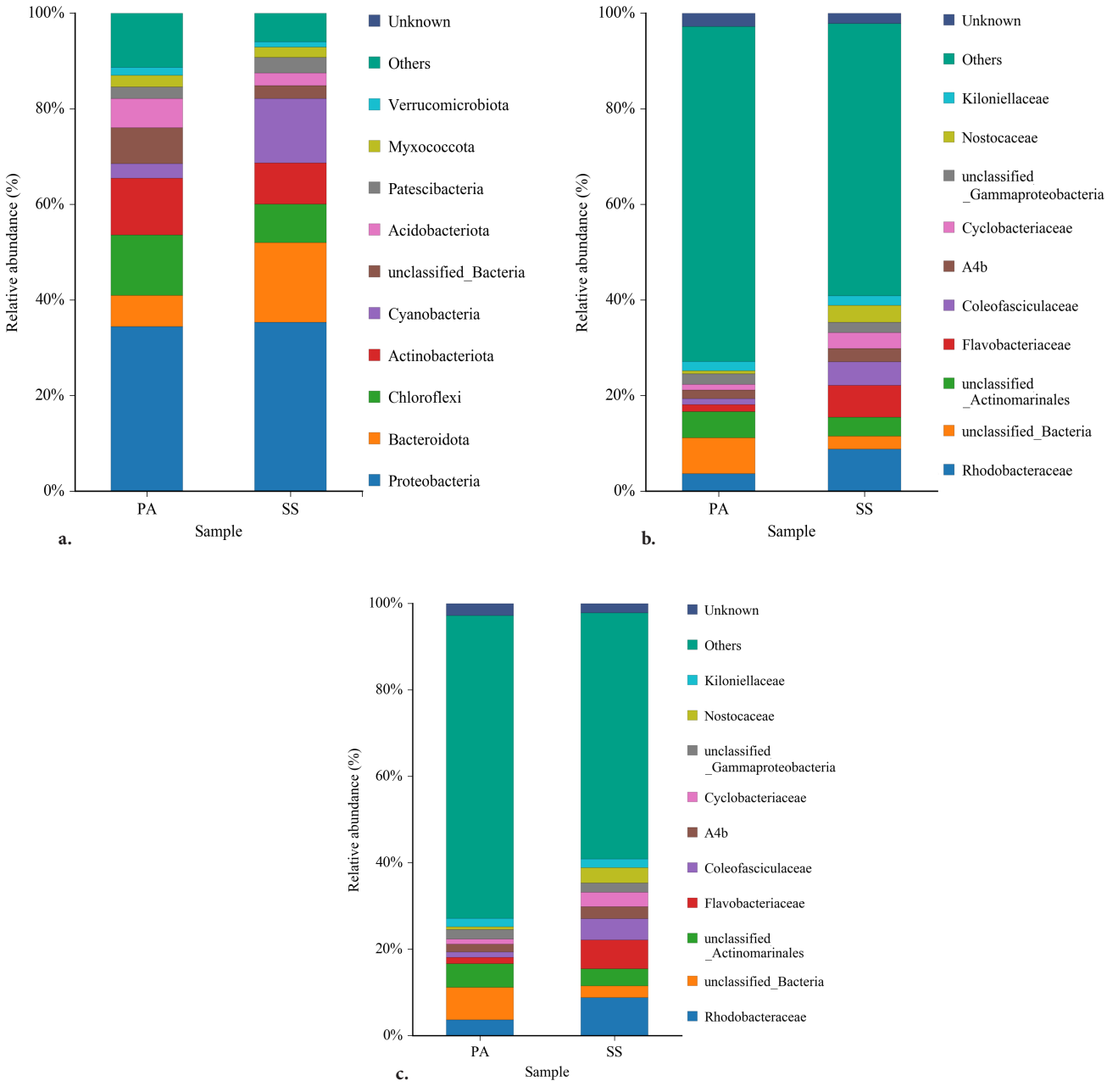

Fig. 2. Bar chart of rhizosphere bacterial community composition for *Phragmites australis* and *Suaeda salsa*. a) Phylum-level bacterial composition; b) Genus-level bacterial composition; c) Family-level bacterial composition: The x-axis denotes sample names. The y-axis represents relative abundance (as a percentage). Colors correspond to distinct taxa, with stacked bars depicting the top 10 taxa by relative abundance at each taxonomic rank.

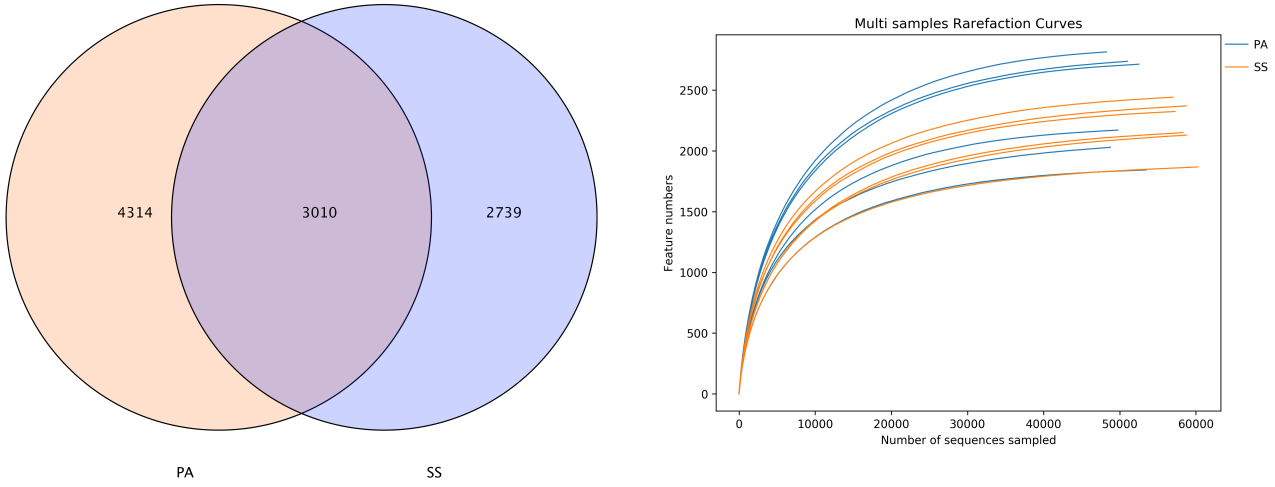

Fig. 3. Core and unique bacterial ASVs and sequencing depth sufficiency between *Phragmites australis and Suaeda salsa* rhizospheres. a) Venn diagram showing the number of shared and unique ASVs between groups; b) Rarefaction curves of observed ASVs. The plateau of curves indicates adequate sequencing depth for microbial diversity analysis.

Table II
Number of ASVs per sample and number of sequences.

Sample ID	**ASVs_Num**	**Seqs_Num**
PA-1	2031	48924
PA-2	2714	52570
PA-3	2816	48397
PA-4	2739	51227
PA-5	2172	49832
PA-6	1844	53546
SS-1	1869	60414
SS-2	2325	57275
SS-3	2443	57159
SS-4	2372	58874
SS-5	2151	58309
SS-6	2132	58982
Total	10063	655509

PA – *Phragmites australis* rhizosphere soil
SS – Suaeda salsa (L.) *Pall.* rhizosphere soil

ing the Student's t-test (independent samples t-test) (R v4.1, stats::t.test) with FDR correction ($q < 0.05$). All samples were rarified to a uniform sequencing depth of 30,000 reads per sample based on rarefaction curve plateau analysis in mothur (v1.22.2) (Wang et al. 2012). Beta diversity analysis was conducted using Principal Coordinates Analysis (PCoA) (Gower 1966) based on Weighted Unifrac distances in QIIME. Statistical significance of sample differences was assessed via PERMANOVA implemented in the vegan R package, with visualizations created in Python. LEfSe analysis was performed to identify discriminative taxa between groups. The analysis first applied the Kruskal-Wallis test ($\alpha = 0.05$) to filter features with significant inter-group differences, followed by Linear Discriminant Analysis (LDA) with a logarithmic score threshold of 4.0. The statistical significance of LDA scores was validated using 1,000 permutations. For functional prediction, PICRUSt2 (v2.3.0) was employed using the phylogenetic placement approach (non-closed reference), where ASVs were inserted into the reference phylogenetic tree (IMG/GTDB) to infer gene families. FAPROTAX (v1.2.6) was used for ecological function annotation based on taxonomic similarity (≥ 97% identity) without closed-reference clustering. Both predictions were performed on the ASV abundance table without OTU clustering. Study area maps were generated in ArcGIS.

Results

Soil physicochemical properties. Analysis of the fundamental physicochemical properties of the rhizosphere soil of the two plants revealed that pH values were stable and did not differ significantly between the *P. australis* and *S. salsa* rhizospheres. In contrast, the electrical conductivity (EC) was significantly higher in the PA rhizosphere compared to the SS rhizosphere (*t*-test, $p < 0.001$).

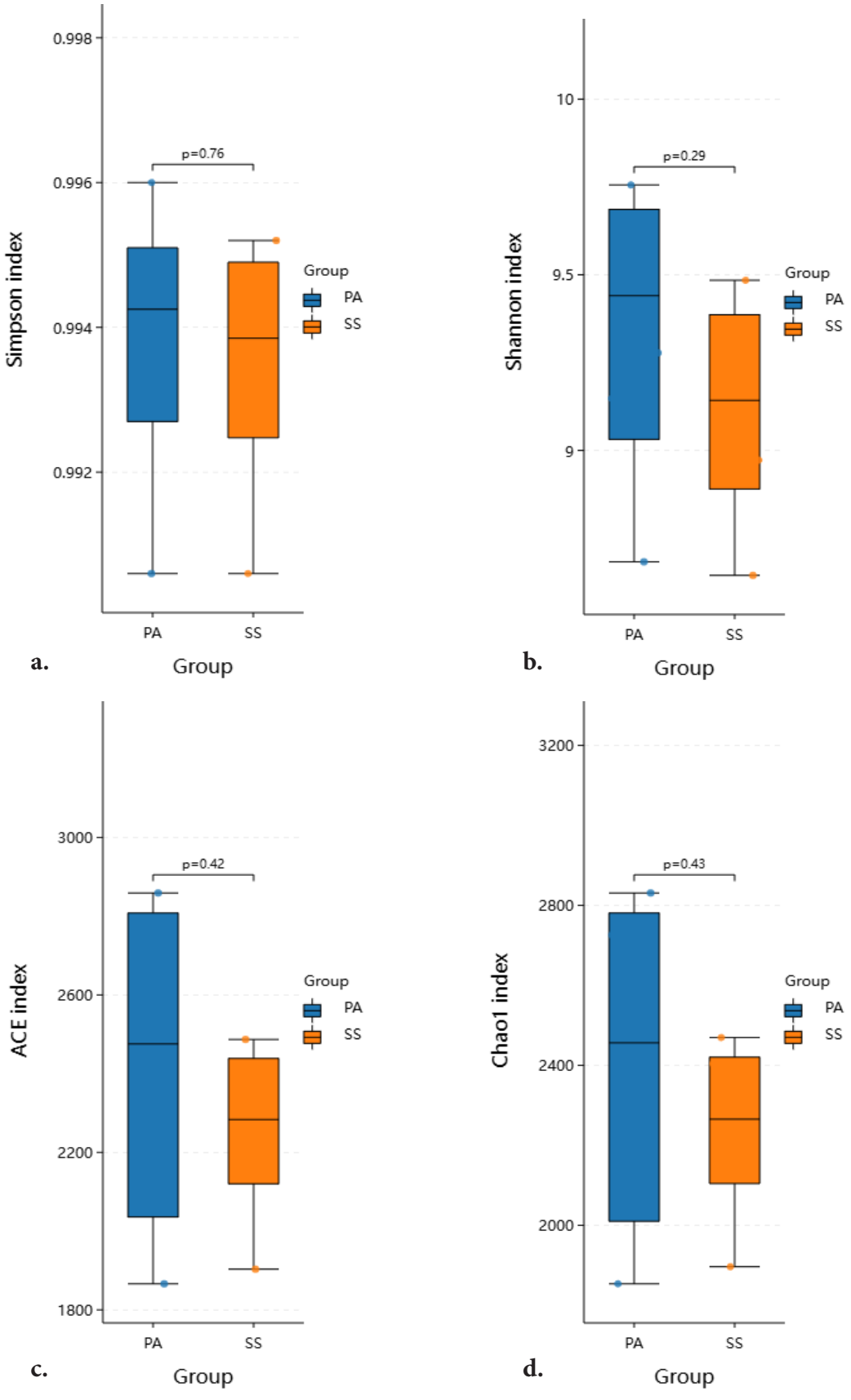

Fig. 4. Alpha diversity of the bacterial microbiota in the rhizosphere of *Phragmites australis* and *Suaeda salsa*. Box plots show the (a) Simpson, (b) Shannon, (c) ACE, and (d) Chao1 indices. The center line represents the median, the box limits indicate the upper and lower quartiles, and the whiskers extend to 1.5× the interquartile range. Outliers are shown as points. Significant differences between groups ($p < 0.05$) are indicated with asterisks and exact p-values.

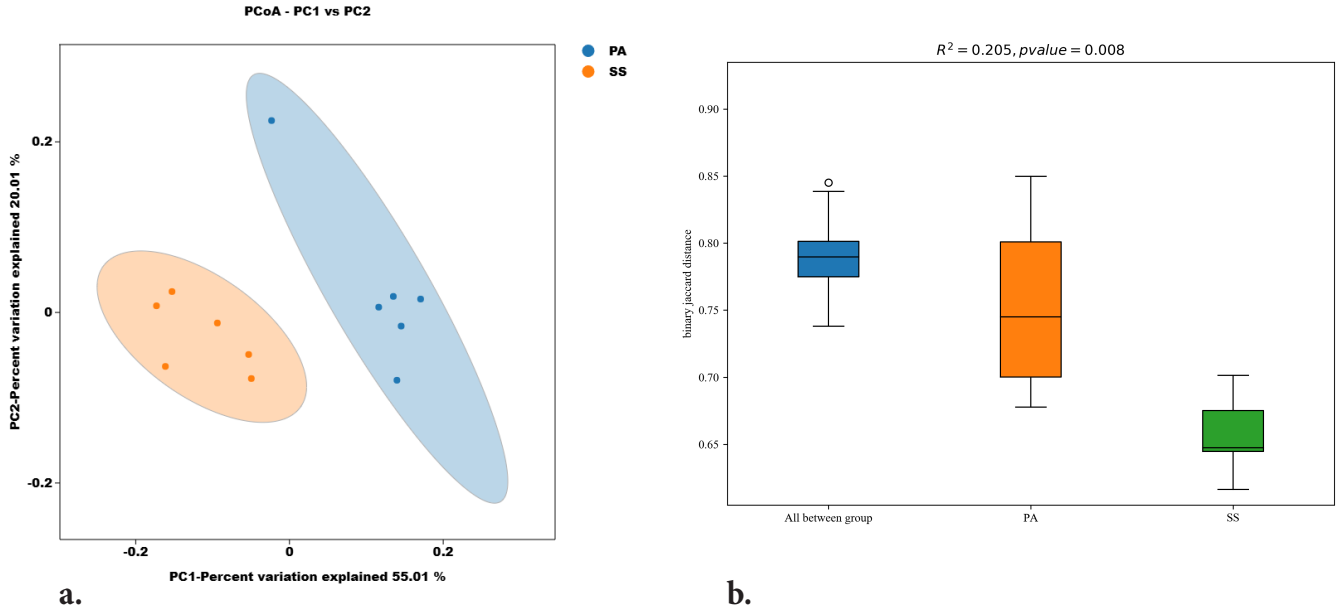

Fig. 5. Beta diversity analysis of rhizosphere bacterial communities. a) Principal coordinates analysis (PCoA) plot. Samples are colored by group, with ellipses showing 95% confidence intervals. Axes show the percent variation explained by each principal component; b) Boxplots comparing between-group and within-group distances.

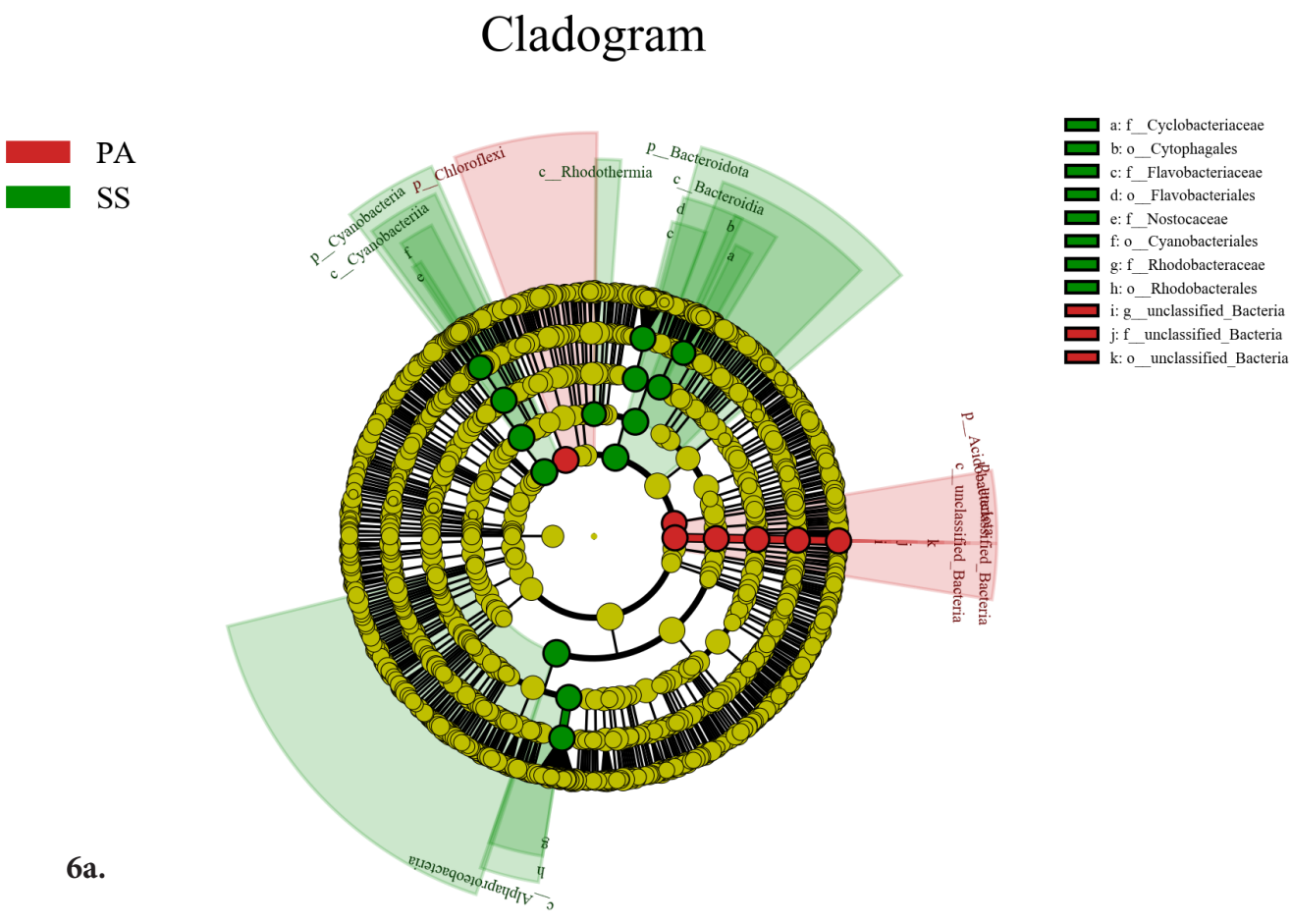

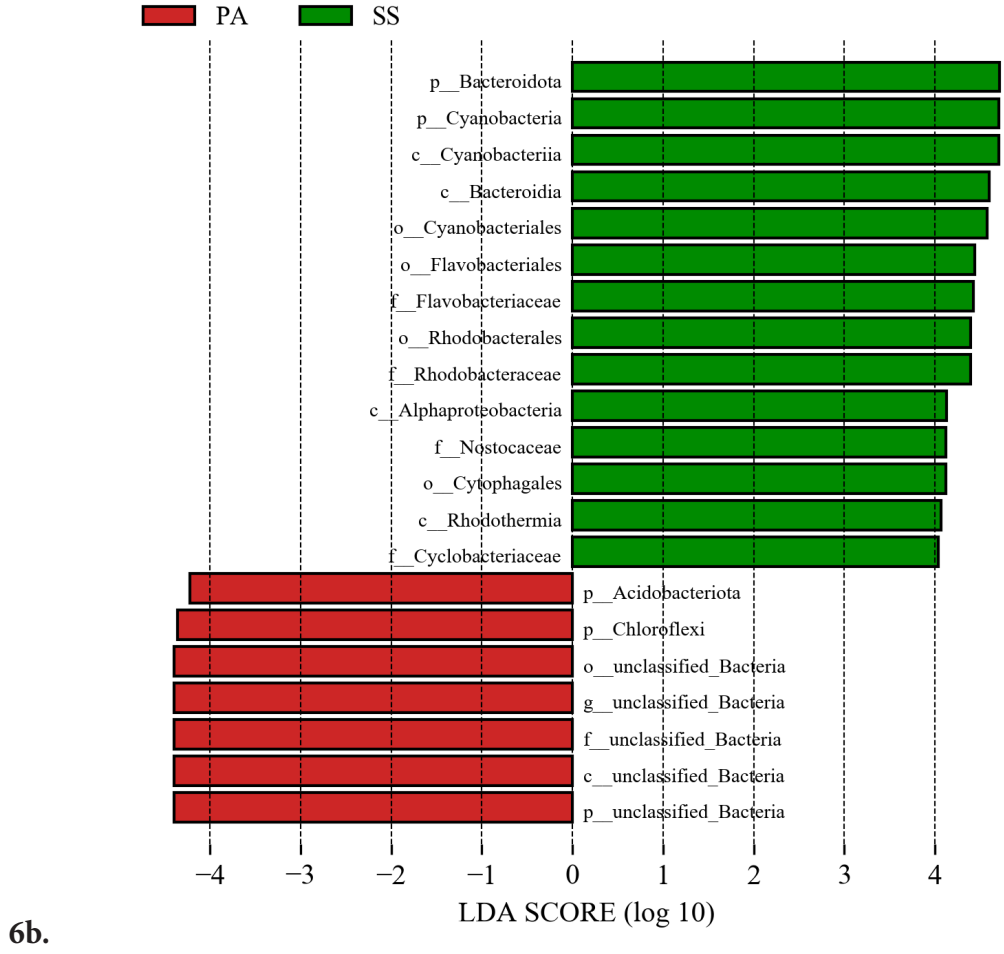

6b.

Fig. 6. LEfSe Analysis Significant microbial differences between the two plants. a) LEfSe analysis phylogenetic tree. The concentric circles radiating from the innermost to the outermost represent taxonomic levels from phylum to species.; b) LDA Value Distribution Bar Chart The vertical axis represents classification units with significant differences between groups. The horizontal axis indicates the degree of difference among classification units, with longer bars signifying greater differences.

Bacteria community structure analysis. Based on species annotation and taxonomic analysis, bar charts of species classification were generated for the top 10 most abundant bacterial species in the rhizosphere soil of common reed and common seepweed. At the phylum level, the dominant bacteria in the PA group are *Proteobacteria, Bacteroidota*, *Chloroflexota, Actinomycetota*, and *Acidobacteriota*. In the SS group, the dominant bacteria are *Proteobacteria*, *Bacteroidota*, *Chloroflexota*, *Actinomycetota*, and *Cyanobacteria*. At the family level, two dominant bacterial families (relative abundance > 1%) were identified in both groups: *unclassified_Coleofasciculaceae*: The relative abundance was 1.05% in the PA group and 3.38% in the SS group, showing a significantly higher abundance in the common seepweed rhizosphere. *unclassified_Unknown_Family*: The relative abundance was 2.48% in the PA group and 1.75% in the SS group, with a higher abundance in the common reed rhizosphere. At the genus level, aside from unclassified species, the dominant genus in both common reed and common seepweed rhizosphere is *Zeaxanthinibacter,* with relative abundances of 0.60% in the PA group and 2.49% in the SS group. Other major unclassified genera include *unclassified_Bacteria*: 7.50% (PA group) and 2.72% (SS group), *unclassified_Actinomarinales*: 4.61% (PA group) and 3.16% (SS group),*unclassified_Gammaproteobacteria*: 2.44% (PA group) and 2.39% (SS group).

In this study, a total of 10,063 bacterial ASVs were obtained across sample groups. The PA group contained 4,314 unique ASVs (42.8%), while the SS group had 2,739 unique ASVs (27.2%). Both groups shared 3,010 ASVs. Rarefaction curves were generated to validate the adequacy of sequencing depth for capturing Bacterial diversity. Curve plateauing indicated sufficient sequence coverage, confirming the robustness of

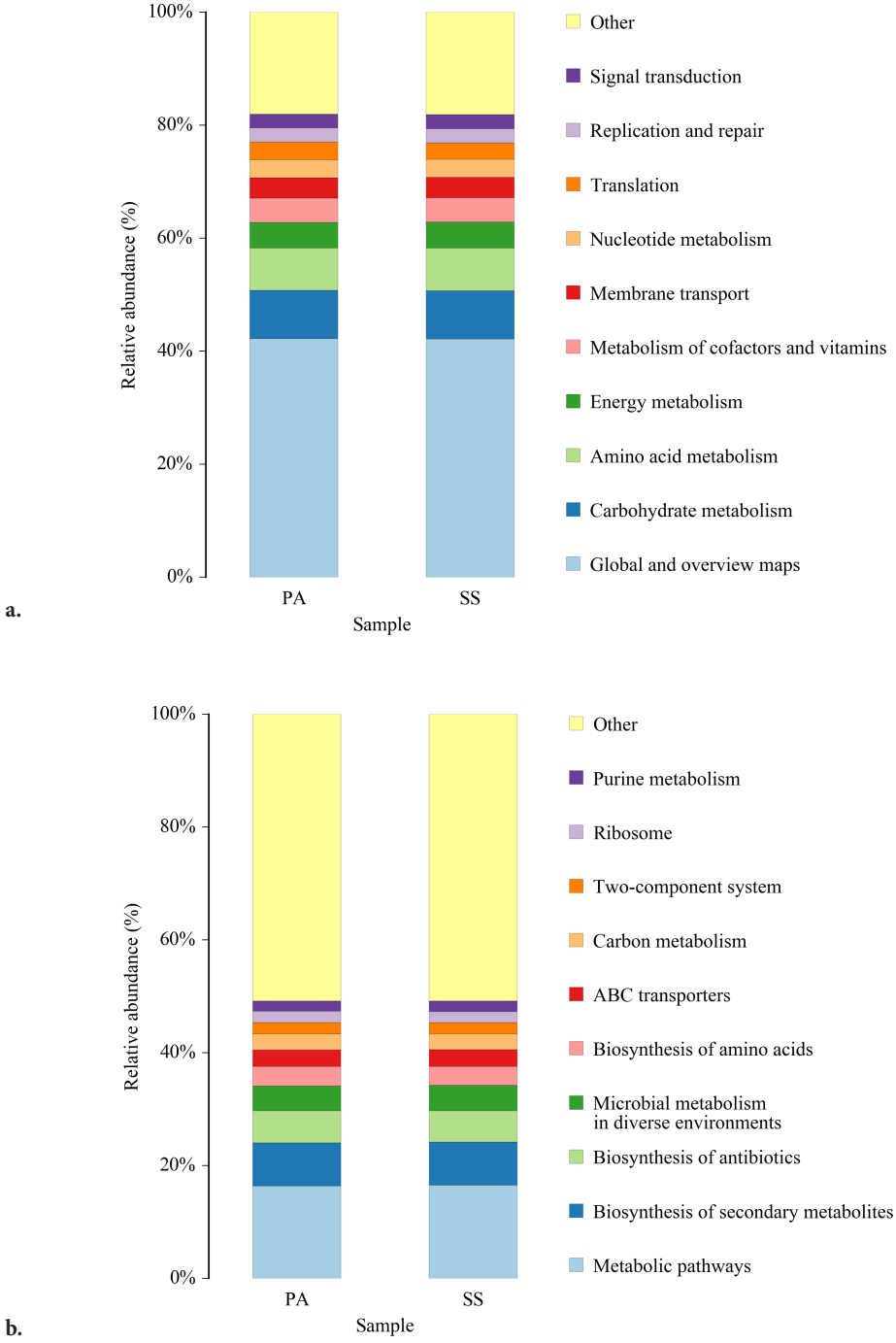

Fig. 7. PICRUSt2 Analysis of *Phragmites australis* and *Suaeda salsa* at Different Functional Levels.
a) KEGG Level 2 functional hierarchy; b) KEGG Level 3 functional hierarchy. The x-axis represents the sample groups, while the y-axis shows the relative abundance (%) of metabolic pathways.

the data for downstream analyses. When the number of randomly selected sequences reaches 10,000, the curve gradually flattens, suggesting that the data are valid.

Analysis of differences in diversity indices among populations. In bacterial community studies, alpha diversity indices are commonly used to characterize the species features of a community. Among these, the Shannon and Simpson indices primarily measure species diversity, while the Chao1 and ACE indices focus on assessing species richness within the community. The results indicated no significant differences in the Simpson index and Shannon index between the PA and SS groups ($p > 0.05$). Similarly, no significant differences were observed in the Chao1 and ACE indexes ($p > 0.05$). The SS groups exhibited a mild upward

trend in key alpha diversity indices relative to the PA group: the Shannon index increased by 5.11% (from 8.41 to 8.84), the Simpson index increased by 0.51% (from 0.987 to 0.992), the Chao1 index increased by 10.20% (from 2027.83 to 2234.58), and the ACE index increased by 10.20% (from 2048.67 to 2257.42). The coverage of all samples was significantly greater than 0.99, indicating that all fragment sequences were detected and that the sequencing results accurately reflect the actual conditions.

Principal Coordinates Analysis (PCoA) was employed to visualize similarities and dissimilarities among samples, providing an intuitive representation of divergence and convergence between distinct bacterial communities. Results demonstrated that PC1 and PC2 accounted for 55.01% and 20.01% of the total β-diversity variation, respectively, in the Weighted Unifrac-based PCoA. Robust separation along the PC1 axis between the PA group (*P. australis*) and SS group (*S. salsa*) was observed with a clear distribution pattern: the PA group exhibited positive PC1 values (mean: 0.1139, range: -0.0233 to 0.1706) while the SS group showed negative PC1 values (mean: -0.1139, range: -0.1730 to -0.0496), Statistical analysis further confirmed that the inter-group difference along PC1 was extremely significant ($p = 0.0001$), whereas no significant difference was detected along the PC2 axis ($p = 0.2385$). PERMANOVA analysis (distance metric: binary_jaccard; permutation method: permanova) further confirmed the statistical significance of inter-group differences. The calculated R^2 value of 0.205 (representing the proportion of variance explained by grouping factors) with higher R^2 values denoting greater separation significance. The statistically significant p-value ($p = 0.008$; $p < 0.05$) validated high analytical reliability.

LEfSe analysis was primarily used to identify differentially expressed biomarkers that were significantly different between sample groups. Analysis of rhizosphere microbes in Common reed and Common seepweed (taxonomic levels: phylum to genus; LDA

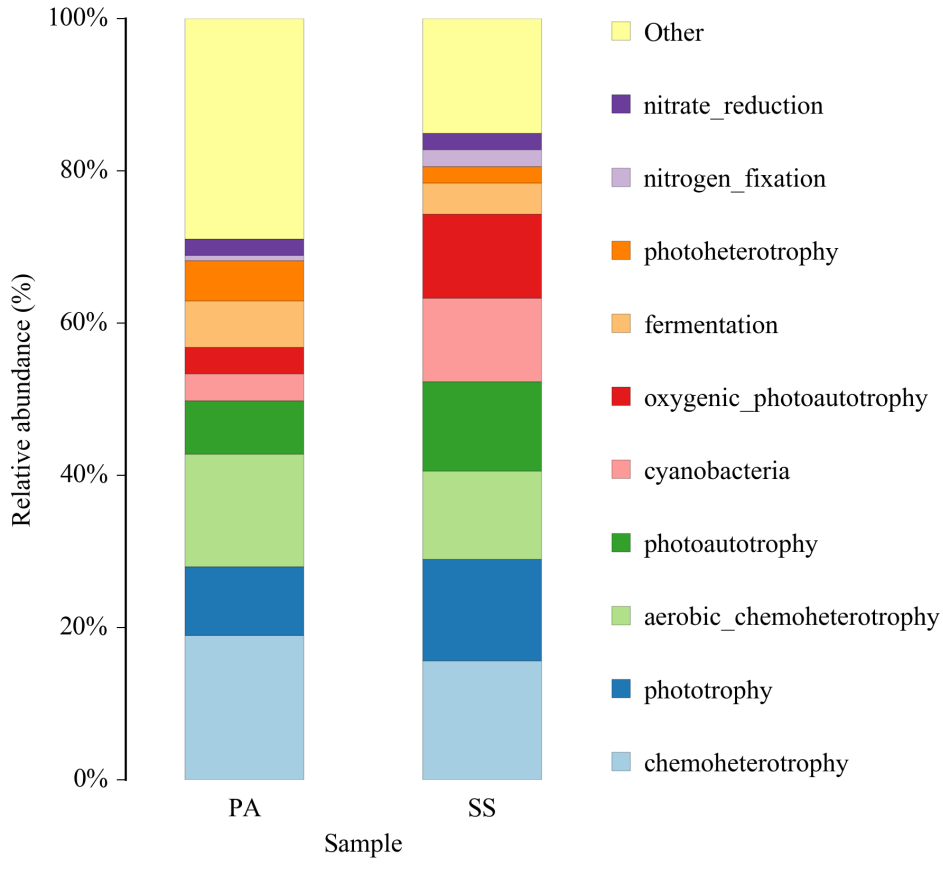

Fig. 8. Differential abundance of predicted ecological functions in the rhizosphere bacterial communities of *Phragmites australis* and *Suaeda salsa*; x-axis, species; y-axis, relative abundance (%) of ecological functions.

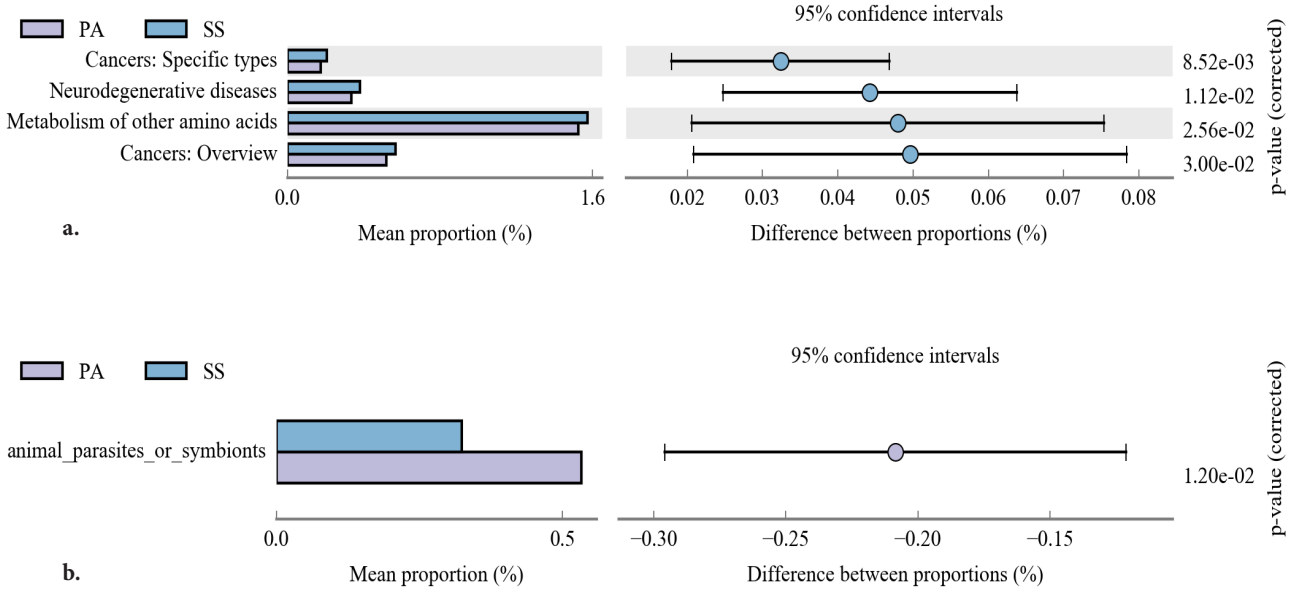

Fig. 9. Differential functional predictions between groups. a) PICRUSt2 and b) FAPROTAX analyses. Colors correspond to sample groups. For each function, the left panel displays relative abundance, the middle panel shows the abundance difference with 95% confidence intervals, and the right panel indicates the *p*-value.

threshold = 4.0) revealed 21 significantly different taxa between the two plant species. Significant biomarkers, excluding unclassified bacteria, included the phyla Acidobacteriota and Chloroflexota in the reed rhizosphere. Biomarkers for Common seepweed comprised: Bacteroidota (phylum), Cyanobacteria (phylum), Cyanobacteria (class), Bacteroidia (class), Alphaproteobacteria (class), Rhodothermia (class), Cyanobacteriales (order), Flavobacteriales (order), Rhodobacterales (order), Cytophagales (order), Flavobacteriaceae (family), Rhodobacteraceae (family), Nostocaceae (family, corrected spelling), Cyclobacteriaceae (family).

Functional prediction of inter-root Bacteria in two plant species. Functional prediction of rhizosphere Bacteria in common reed and common seepweed was conducted using PICRUSt2, focusing on the top 10 functional categories by relative abundance under KEGG Level 2 classification. This analysis revealed that both plant rhizospheres exhibited similar functional profiles with comparable abundances. The predominant metabolic pathway-related functions included global and overview maps (the most dominant function), carbohydrate metabolism, amino acid metabolism, energy metabolism, metabolism of cofactors and vitamins, membrane transport, and nucleotide metabolism; genetic information processing-related functions comprised translation, replication, and repair, while environmental information processing-related functions featured signal transduction.

Further analysis of the top 10 most abundant KEGG Level 3 functional categories via PICRUSt2 prediction revealed functional congruence, with comparable abundances between common reed (*P. australis*) and common seepweed (*S. salsa*) rhizospheres. Metabolic pathway-related functions included metabolic pathways (dominant function), biosynthesis of secondary metabolites, biosynthesis of antibiotics, bacteria metabolism in diverse environments, biosynthesis of amino acids, carbon metabolism, and purine metabolism; environmental information processing-related functions comprised two-component system; genetic information processing-related functions featured ribosome; cellular process-related functions involved ABC transporters.

FAPROTAX analysis of the top 10 ecological functions in the rhizospheres of common reed and seepweed revealed shared functional profiles with divergent relative abundances. Functions included: photosynthetic carbon/nitrogen fixation (oxygenic_photoautotrophy: PA 3.53%, SS 11.02%; cyanobacteria: PA 3.53%, SS 11.02%); mixotrophic metabolism (photoautotrophy:

PA 6.99%, SS 11.7%; photoheterotrophy: PA 5.25%, SS 2.16%); aerobic organic matter degradation (aerobic_chemoheterotrophy: PA 14.79%, SS 11.58%); anaerobic energy backup (fermentation: PA 6.09%, SS 4.08%); nitrogen cycling (nitrate_reduction: PA 2.18%, SS 2.13%; nitrogen_fixation: PA 0.69%, SS 2.21%). The top-tier functional categories, phototrophy (PA 9%, SS 13.37%) and chemoheterotrophy (PA 18.99%, SS 15.61%), hierarchically encompass the sub-functions above, with phototrophy comprising photoautotrophy and photoheterotrophy. In contrast, chemoheterotrophy includes aerobic chemoheterotrophy and fermentation.

Predicting functional differences in rhizosphere bacteria between two plant species. Analysis of the top 30 most abundant KEGG pathways (level 2) revealed limited functional divergence between the two plant species. Microbial functional profiles were largely characterized by conserved core metabolism, with only three pathways showing statistically significant differences (FDR-corrected $p < 0.05$), all of which were enriched in common seepweed (SS). Two additional pathways approached significance, though all differentially abundant categories exhibited modest effect sizes. At a finer functional resolution (level 3), none of the top 30 KEGG pathways differed significantly between groups. Similarly, FAPROTAX profiling of the top 30 ecological functions identified only one significant group difference: the relative abundance of animal_parasites_or_symbionts was higher in common reed (PA; 0.53%) than in common seepweed (SS; 0.32%; corrected p = 0.012). No other functions have achieved statistical significance.

Discussion

Analysis of rhizosphere physicochemical properties revealed that although both plants grew in soil with a consistent pH background ($p > 0.05$), they created markedly different rhizosphere microenvironments. The common reed rhizosphere showed significantly higher electrical conductivity ($p < 0.001$), aligning with its salt-exclusion strategy by accumulating salts in the rhizosphere to prevent excessive shoot uptake. In contrast, the lower EC in common seepweed rhizosphere corresponds to its salt-secreting/diluting physiological mechanism. This plant-driven divergence in rhizosphere chemical conditions is likely a key driver of the significant differences in their rhizosphere microbial community structures. These findings demonstrate that, in a shared soil reservoir, host plant species are the primary factor shaping the rhizosphere microenvironment.

Soil bacteria play pivotal roles in material cycling and signal transduction within the rhizosphere (Yang et al. 2025), critically contributing to plant growth promotion, nutrient acquisition, and maintenance of plant health (Mukhtar et al. 2025). Rhizosphere bacteria community composition and functionality are fundamental to these processes. In the context of increasingly severe global coastal salinization, understanding plant-microbe interactions is particularly significant for the conservation and restoration of coastal ecosystems. This study analyzed bacterial communities and their functions in the rhizosphere environments of common reed and common seepweed by extracting rhizosphere soil DNA and using 16S rRNA high-throughput sequencing. Results revealed a distinctive pattern of structural differentiation but functional convergence between the two plant-associated microbiomes, consistent with prior research (Louca et al. 2018). Overall, the rhizosphere microbiomes of the two plant species exhibited a clear pattern of structural differentiation despite functional convergence. Alpha diversity indices showed no significant differences between species, whereas beta diversity analysis based on Weighted Unifrac distance revealed significant compositional divergence (P = 0.008). This structural distinction was further supported by LEfSe analysis, which identified 21 differentially abundant taxa. In contrast, both PICRUSt2 functional predictions and FAPROTAX ecological profiling indicated highly similar functional profiles between the two rhizospheres.

The absence of differences in alpha diversity alongside significant PCoA separation may arise because both plants inhabit the same environment, yet differ in salt tolerance mechanisms and root exudates. In addition, rhizosphere samples were collected during the early growth stage (Liu et al. 2023), when recruitment strategies—specifically the enrichment or suppression of specific bacterial taxa—can diverge (Walters and Martiny 2020; Zverev et al. 2021). Alternatively, the unique salinized soils of Chenier Islands may exert a more substantial community-shaping effect than root-mediated selection (Ding et al. 2023; Gao et al. 2020). The lack of alpha-diversity differences indicates that the two rhizospheres possess similar capacities to host bacteria (Wei et al. 2020), providing stable nich-

es for microbes even under salt stress. This finding provides important insights into the mechanisms that maintain stability in fragile coastal wetland ecosystems such as the Chenier Islands. The pronounced PCoA dissimilarity suggests species turnover—replacement of taxa. At the same time, functional roles are retained, allowing plants to eliminate sensitive microbes and recruit functionally equivalent microbes to cope with environmental pressures (Huang et al. 2024).

Functional redundancy enables the rhizosphere microbiomes of the two plants to maintain similar functional potential despite differences in community composition (Louca et al. 2018). This implies that even if the bacterial community shifts, the overall functionality can remain stable provided that the keystone functional guides persist or are compensated by other taxa with equivalent functions. Under the dual pressures of sea-level rise and intensifying salinization in global coastal zones, this functional redundancy mechanism provides a micro-level explanation for the maintenance of coastal vegetation ecosystem resilience.

LEfSe analysis identified Acidobacteriota as a differential biomarker in the common reed rhizosphere, primarily associated with carbohydrate metabolism and Global and overview maps pathways, consistent with prior research (Gonçalves et al. 2024). This phylum facilitates plant adaptation to hypersaline conditions on the Chenier Islands by decomposing complex soil carbohydrates, releasing sugars, small-molecule compounds, and antioxidants (Wang et al. 2025). Concurrently, it coordinates diverse metabolic activities to drive carbon, nitrogen, and sulfur cycling, thereby enhancing soil quality in the rhizosphere (Douglas et al. 2020). Meanwhile, Chloroflexota predominantly performs Energy metabolism and amino acid metabolism (Bovio-Winkler et al. 2023), participating in glycolytic and TCA cycle pathways to supply energy, carbon, and nitrogen to plant roots. It further regulates intracellular redox homeostasis (Liu et al. 2022) and osmoregulation, strengthening salt-stress resilience (Ingrisano et al. 2023). In common seepweed, differential biomarkers predominantly comprised Cyanobacteria, Proteobacteria, and Bacteroidota. Their core functional pathways encompassed Global and overview maps, Energy metabolism, and Amino acid metabolism. Research indicates these bacteria facilitate plant growth and enhance salt-stress resilience through photosynthesis, carbon/nitrogen fixation, phytohormone secretion, organic matter decomposition, and nutrient cycling (Gao et al. 2019; Kollmen and Strieth 2022; Ravanbakhsh et al. 2019).

The results indicate that both common reed and common seepweed prioritize functional rather than taxonomic composition in their rhizosphere microbiomes. By secreting specific root exudates, the plants recruit microbes that possess the required functional traits (Sasse et al. 2018) to meet the metabolic demands of coping with salt stress, irrespective of the exact species that provide these functions. This confirms that plants are the primary architects of their rhizosphere bacterial communities, a conclusion consistent with previous findings (Yang et al. 2025). In the typical intertidal ecosystem of the Chenier Islands, plants effectively maintain survival and reproduction in highly saline environments through function-oriented microbial recruitment strategies, providing theoretical references for vegetation restoration in similar coastal ecosystems worldwide.

PICRUSt2 and FAPROTAX—functional prediction tools based on distinct principles and databases—revealed convergent metabolic potentials in the rhizosphere microbiomes of common reed and seepweed. While PICRUSt2 predictions showed identical functional categories with highly similar relative abundances at both KEGG Levels 2 and 3, FAPROTAX ecological profiling, despite confirming functional congruence, revealed quantitative disparities in relative abundances. This outcome significantly reinforces the hypothesis that plant-driven selection of rhizosphere microbes prioritizes functional convergence over taxonomic identity. FAPROTAX predicts bacterial community functions based on taxonomic information and known ecological classifications (Sansupa et al. 2021). When the composition and structure of the rhizosphere microbiota differ between the two plants, this may lead to differences in the relative abundance of functions (Guo et al. 2025; Li et al. 2025), even if they can perform similar functions. Thus, differences in the relative abundance of functions in the FAPROTAX analysis do not undermine the validity of the conclusion above. This also confirms that functional redundancy is a vital foundation for ecosystem stability (Biggs et al. 2020). When the core functional microbes of common reed and common seepweed are reduced due to environmental factors, other species with the same functions can compensate and maintain functional output (Louca et al. 2018). This is crucial for their adaptation to the saline stress of the Chenier Islands and various environmental changes. With increasing environmental uncertainties in coastal zones due to global climate change, revealing this functional redundancy mech-

anism has profound implications for predicting and regulating functions of salinized ecosystems, while also offering new perspectives for bioremediation strategies in coastal saline-alkali lands.

The widespread functional redundancy observed in this study, in which distinct microbial taxa support overlapping metabolic functions, carries profound ecological implications for plant adaptation in dynamic saline environments. This mechanism provides halophytes with functional resilience, ensuring the stability of critical processes, such as nutrient mineralization and stress hormone regulation, even when microbial community composition fluctuates due to environmental disturbances. For the host plants, this means that their adaptation does not rely on the presence of specific, potentially sensitive microbial species, but rather on a buffered, functionally versatile microbiome. Consequently, common seepweed can depend on a consistent supply of fixed nitrogen from various photoautotrophic taxa, while common reed can secure its carbon and energy needs through multiple heterotrophic pathways. This ecological strategy effectively decouples plant fitness from taxonomic volatility, allowing both species to thrive under the saline-alkaline stresses of the Chenier Islands by maintaining core physiological functions through diverse yet functionally equivalent microbial partnerships.

The observed functional convergence despite taxonomic divergence suggests the operation of profound ecological and evolutionary mechanisms that shape the rhizosphere microbiome in this saline environment (Li et al. 2024). First, environmental filtering imposed by the pervasive salt stress on Chenier Islands serves as a primary selective force, constraining the total repertoire of metabolically viable functions. The high salinity acts as a filter, permitting only microorganisms with specific genetic traits for osmolyte synthesis, ion homeostasis, and salt-tolerant enzymes to establish and function, thereby limiting the range of possible functional profiles. Second, functional redundancy, the existence of multiple phylogenetically distinct taxa capable of performing the same biochemical process, provides the necessary 'raw material' for this convergence (Louca et al. 2018). This redundancy allows each plant host to recruit from a common regional species pool but arrive at distinct taxonomic assemblages that are functionally equivalent. Most critically, the convergence is likely driven by host-mediated selection for key functions. Rather than selecting for specific microbial taxa *per se*, the plants appear to exert selective pressure on microorganisms through their root exudates that can provide host-beneficial services (Pantigoso et al. 2022; Yetgin 2023). For common reed, this may manifest as a strong selection for heterotrophic degraders to mineralize organic matter (Guan et al. 2017), whereas for common seepweed, the selection likely favors phototrophic and nitrogen-fixing partners (Song et al. 2022). In essence, the plants address similar challenges of nutrient acquisition and stress tolerance in a saline habitat by cultivating microbial communities that provide these essential services, regardless of their taxonomic identity. This represents a sophisticated form of ecosystem-level optimization, prioritizing functional stability over taxonomic composition to ensure resilience in a dynamic intertidal environment.

The observed pattern of functional convergence amidst taxonomic divergence finds strong parallels in other saline ecosystems yet highlights the unique rhizosphere mediation by coastal halophytes. In inland salinized grasslands, halophytes create "saline fertile islands" that enrich functional genes essential for nutrient cycling, demonstrating how plant activity directly enhances microbial metabolic capabilities (Liang et al. 2025; Zhao et al. 2024). Similarly, the temporal dynamics of microbial functional genes in reclaimed salinized farmland reveal that community function can stabilize despite compositional changes (Yin et al. 2024), echoing the functional redundancy we observed in the Chenier Islands. However, our study reveals a more specialized mechanism: host-specific functional guild selection. While studies of saline lake sediments show that bacterial communities adapt to environmental stress through functional gene shifts (Yang et al. 2022), our findings demonstrate that common reed and common seepweed actively recruit distinct taxonomic groups to maintain convergent functions—a strategy more targeted than the broader environmental filtering observed in bulk soils. This represents a refined ecological strategy in which coastal halophytes in shell-sand matrices optimize functional acquisition through taxonomic flexibility, thereby ensuring ecosystem resilience amid increasing salinization pressures.

Although rhizosphere microbes in intertidal saline systems have been extensively investigated, existing studies have predominantly focused on either "community structure description" or "single function-

al genes," leaving the "structure-function" coupling mechanism and the differentiation of plant energy strategies unresolved. This study is the first in Chenier Island sedimentary environments to integrate ASV-level structural differences with PICRUSt2/FAPROTAX functional profiling and statistical testing, revealing how *P. australis* and *S. salsa* achieve niche separation through contrasting "photoautotrophy-nitrogen fixation" versus "chemoheterotrophy-nitrate reduction" pathways. We propose a rhizosphere model of "structural differentiation but functional convergence". These findings provide new perspectives for plant-microbe synergistic adaptation theory in saline lands and offer insights applicable to other coastal wetlands for optimizing vegetation restoration and carbon sequestration management.

This study has several limitations that should be considered. First, we acknowledge the inherent constraints of the 16S rRNA amplicon sequencing approach, which, unlike shotgun metagenomics, provides limited phylogenetic resolution and cannot directly access the full functional gene repertoire of microbial communities (Zhu et al. 2022). The functional profiles derived from PICRUSt2 and FAPROTAX are probabilistic predictions based on taxonomic data and existing databases, reflecting metabolic potential rather than actual microbial activity. These predictions are further constrained by the completeness and annotation accuracy of the reference databases themselves, which may not fully capture the unique genetic potential of environmental microbes. Experimental validation is needed to confirm their ecological relevance. Second, the rhizosphere samples were collected during the early plant growth stage and thus may not fully represent stabilized microbial communities in later developmental phases. Third, although the stark contrast in microbial communities between the two plant species—grown in immediate proximity and thus sharing the same soil pool—strongly suggests host-specific selection, the absence of bulk-soil controls prevents definitive partitioning of the rhizosphere microbiota into "soil-derived" and "plant-recruited" components. Future studies incorporating paired bulk soil sampling will be essential to precisely quantify plant enrichment effects in this ecosystem. Finally, as bacterial assembly is influenced by multiple factors, this study focused primarily on plant-specific effects, and other potential influences warrant further investigation.

Conclusions

In summary, this study demonstrates that although common reed and common seepweed recruit phylogenetically distinct rhizosphere bacterial communities, these assemblages exhibit functional convergence under saline conditions. The observed niche partitioning—photoautotrophic dominance in seepweed versus chemoheterotrophic specialization in reed—reflects divergent microbial recruitment strategies, yet both pathways ultimately support plant adaptation through complementary mechanisms. This pattern of "structural differentiation but functional convergence" highlights the importance of functional redundancy in maintaining ecosystem stability under environmental stress, indicating that different bacterial community compositions can achieve analogous ecological functions in helping plants adapt to saline environments. However, it should be noted that the functional roles attributed to bacterial taxa are based on predictive tools (PICRUSt2 and FAPROTAX) rather than experimental validation. Future work incorporating metatranscriptomics or enzyme activity assays will be essential to empirically verify these putative functions and further elucidate the mechanistic basis of plant-microbe interactions in saline ecosystems. Additionally, future research should explore how these plant-specific microbial recruitment strategies vary across seasonal dynamics and environmental gradients. From an applied perspective, our findings provide a microbial ecological basis for optimizing vegetation restoration strategies in coastal saline lands by leveraging the complementary functions of different halophyte species.

Data availability statement

Raw sequence data were deposited in the Sequence Read Archive (SRA) database of NCBI under BioProject number PRJNA1301057 and Biosample numbers SAMN50434325-SAMN50434336.

Author contributions

Conceptualization B.Z.; methodology B.Z.; software B.Z.; sample collection B.Z., J.Y.; validation S.S., J.W. and X.S.; formal analysis J.L., L.L.; writing—original draft preparation B.Z. and J.Y.; writing—review and editing B.Z., S.S. and J.W. All authors have read and agreed to the published version of the manuscript.

Funding

The Taishan Industrial Experts Program, and Science and Technology Support Plan for Youth Innovation of Colleges and Universities in Shandong Province (2022KJ088).

Conflict of interest

The authors do not report any financial or personal connections with other persons or organizations, which might negatively affect the contents of this publication and/or claim authorship rights to this publication.

Literature

Biggs CR, **Yeager LA**, **Bolser DG**, **Bonsell C**, **Dichiera AM**, **Hou Z**, **Erisman BE**. 2020. Does functional redundancy affect ecological stability and resilience? A review and meta-analysis. *Ecosphere*. 11(7):e03184. https://doi.org/10.1002/ecs2.3184

Bolger AM, **Lohse M**, **Usadel B**. 2014. Trimmomatic: a flexible trimmer for Illumina sequence data. *Bioinformatics*. 30(15):2114–2120. https://doi.org/10.1093/bioinformatics/btu170

Bolyen E, **Rideout JR**, **Dillon MR**, **Bokulich NA**, **Abnet CC**, **Al-Ghalith GA**, **Caporaso JG**. 2019. Reproducible, interactive, scalable and extensible microbiome data science using QIIME 2. *Nat Biotechnol*. 37(8):852–857. https://doi.org/10.1038/s41587-019-0209-9

Bovio-Winkler P, **Guerrero LD**, **Erijman L**, **Oyarzúa P**, **Suárez-Ojeda ME**, **Cabezas A**, **Etchebehere C**. 2023. Genome-centric metagenomic insights into the role of Chloroflexi in anammox, activated sludge and methanogenic reactors. *BMC Microbiol*. 23:45. https://doi.org/10.1186/s12866-023-02765-5

Callahan BJ, **McMurdie PJ**, **Rosen MJ**, **Han AW**, **Johnson AJA**, **Holmes SP**. 2016. DADA2: high-resolution sample inference from Illumina amplicon data. *Nat Methods*. 13(7):581–583. https://doi.org/10.1038/nmeth.3869

Cao C, **Su F**, **Song F**, **Yan H**, **Pang Q**. 2022. Distribution and disturbance dynamics of habitats suitable for *Suaeda salsa*. *Ecol Indic*. 140:108984. https://doi.org/10.1016/j.ecolind.2022.108984

Chapman SK, **Newman GS**. 2010. Biodiversity at the plant–soil interface: microbial abundance and community structure respond to litter mixing. *Oecologia*. 162(3):763–769. https://doi.org/10.1007/s00442-009-1498-3

Chen C, **Wang Y**, **Yang L**, **Min Y**, **Yue K**, **Lu S**, **Zhang L**. 2025. The impact of litter from different belowground organs of *Phragmites australis* on microbial-mediated soil organic carbon accumulation in a lacustrine wetland. *Microorganisms*. 13(5):1146. https://doi.org/10.3390/microorganisms13051146

Chen Y, **Kong D**, **Wang Z**, **Liu J**, **Wang L**, **Dai K**, **Cao J**. 2025. A wheat CC-NBS-LRR protein Ym1 confers WYMV resistance by recognizing viral coat protein. *Nat Commun*. 16:3630. https://doi.org/10.1038/s41467-025-58816-0

Čížková H, **Lukavská J**. 1999. Rhizome age structure of three populations of *Phragmites australis* (Cav.) Trin. ex Steud.: biomass and mineral nutrient concentrations. *Folia Geobot*. 34(2):209–220. https://doi.org/10.1007/BF02913396

Ding Y, **Geng Y**, **Zhou W**, **Li D**. 2023. Habitat-specific environmental factors regulate the spatial variability of biological soil crust microbial communities on the Qinghai-Tibet Plateau. *Sci Total Environ*. 901:165937. https://doi.org/10.1016/j.scitotenv.2023.165937

Douglas GM, **Maffei VJ**, **Zaneveld JR**, **Yurgel SN**, **Brown JR**, **Taylor CM**, **Langille MGI**. 2020. PICRUSt2 for prediction of metagenome functions. *Nat Biotechnol*. 38(6):685–688. https://doi.org/10.1038/s41587-020-0548-6

Edgar RC, **Haas BJ**, **Clemente JC**, **Quince C**, **Knight R**. 2011. UCHIME improves sensitivity and speed of chimera detection. *Bioinformatics*. 27(16):2194–2200. https://doi.org/10.1093/bioinformatics/btr381

Edgar RC. 2013. UPARSE: highly accurate OTU sequences from microbial amplicon reads. *Nat Methods*. 10(10):996–998. https://doi.org/10.1038/nmeth.2604

Gao GF, **Peng D**, **Tripathi BM**, **Zhang Y**, **Chu H**. 2020. Distinct community assembly processes of abundant and rare soil bacteria in coastal wetlands along an inundation gradient. *mSystems*. 5(6):e01150-20. https://doi.org/10.1128/msystems.01150-20

Gao S, **Pan L**, **Huang F**, **Song M**, **Tian C**, **Zhang M**. 2019. Metagenomic insights into the structure and function of intestinal microbiota of the farmed Pacific white shrimp (*Litopenaeus vannamei*). *Aquaculture*. 499:109–118. https://doi.org/10.1016/j.aquaculture.2018.09.026

Gonçalves OS, **Fernandes AS**, **Tupy SM**, **Ferreira TG**, **Almeida LN**, **Creevey CJ**, **Santana MF**. 2024. Insights into plant interactions and the biogeochemical role of the globally widespread *Acidobacteriota* phylum. *Soil Biol Biochem*. 192:109369. https://doi.org/10.1016/j.soilbio.2024.109369

Gower JC. 1966. Some distance properties of latent root and vector methods used in multivariate analysis. *Biometrika*. 53(3–4):325–338. https://doi.org/10.1093/biomet/53.3-4.325

Guan B, **Yu J**, **Hou A**, **Han G**, **Wang G**, **Qu F**, **Wang X**. 2017. The ecological adaptability of *Phragmites australis* to interactive effects of water level and salt stress in the Yellow River Delta. *Aquat Ecol*. 51(1):107–116. https://doi.org/10.1007/s10452-016-9602-3

Guo HB, **Zhao JC**, **Liu WY**, **Bi YD**, **Sibirina LA**, **Yu XD**. 2025. Microbiome analysis for artificially establishing the symbiotic relationship between *Hebeloma hiemale* and *Quercus mongolica*. *Sci Rep*. 15:1–12. https://doi.org/10.1038/s41598-025-03963-z

Huang X, **Zhou W**, **Zhang Y**, **Yang Q**, **Yang B**, **Liang T**, **Dong J**. 2024. Keystone PGPR ecological effect: an inoculation case study of diazotrophic *Novosphingobium* sp. N034 on mangrove plant *Kandelia obovata*. *Appl Soil Ecol*. 202:105567. https://doi.org/10.1016/j.apsoil.2024.105567

Huang Y, **Zhai L**, **Chai X**, **Liu Y**, **Lv J**, **Pi Y**, **Wang Y**. 2024. *Bacillus* B2 promotes root growth and enhances phosphorus absorption in apple rootstocks by affecting MhMYB15. *Plant J*. 119(4):1880–1899. https://doi.org/10.1111/tpj.16893

Ingrisano R, **Tosato E**, **Trost P**, **Gurrieri L**, **Sparla F**. 2023. Proline, cysteine and branched-chain amino acids in abiotic stress response of land plants and microalgae. *Plants*. 12(19):3410. https://doi.org/10.3390/plants12193410

Juneau KJ, **Tarasoff CS**. 2013. The seasonality of survival and subsequent growth of common reed (*Phragmites australis*) rhizome fragments. *Invasive Plant Sci Manag*. 6:79–86. https://doi.org/10.1614/IPSM-D-12-00051.1

Kollmen J, **Strieth D**. 2022. The beneficial effects of cyanobacterial co-culture on plant growth. *Life*. 12(2):223. https://doi.org/10.3390/life12020223

Kraepiel AML, **Bellenger JP**, **Wichard T**, **Morel FMM**. 2009. Multiple roles of siderophores in free-living nitrogen-fixing bacteria. *Biometals*. 22:573–581. https://doi.org/10.1007/s10534-009-9222-7

Li J, **Zhang H**, **Long S**, **Li W**, **Wang T**, **Yu J**, **Cheng Y**. 2025. DNA metabarcode analyses reveal similarities and differences in plant microbiomes of industrial hemp and medicinal *Cannabis* in China. *Front Microbiol*. 16:1524703. https://doi.org/10.3389/fmicb.2025.1524703

Li M, **Zhou W**, **Sun M**, **Shi W**, **Lun J**, **Zhou B**, **Gao Z**. 2024. Decoupling soil community structure, functional composition, and nitrogen metabolic activity driven by salinity in coastal wetlands. *Soil Biol Biochem*. 198:109547. https://doi.org/10.1016/j.soilbio.2024.109547

Li R, **Jiao H**, **Sun B**, **Song M**, **Yan G**, **Bai Z**, **Hu Q**. 2024. Understanding salinity-driven modulation of microbial interactions: rhizosphere versus edaphic microbiome dynamics. *Microorganisms*. 12(4):683. https://doi.org/10.3390/microorganisms12040683

Liang M, **Wu Y**, **Jiang Y**, **Zhao Z**, **Yang J**, **Liu G**, **Xue S**. 2025. Microbial functional genes play crucial roles in enhancing soil nutrient availability of halophyte rhizospheres in salinized grasslands. *Sci Total Environ*. 958:178160. https://doi.org/10.1016/j.scitotenv.2024.178160

Liu R, **Wei X**, **Song W**, **Wang L**, **Cao J**, **Wu J**, **Fang J**. 2022. Novel *Chloroflexi* genomes from the deepest ocean reveal metabolic strategies for the adaptation to deep-sea habitats. *Microbiome*. 10:75. https://doi.org/10.1186/s40168-022-01263-6

Liu S, **Gao J**, **Wang S**, **Li W**, **Wang A**. 2023. Community differentiation of rhizosphere microorganisms and their responses to environmental factors at different development stages of medicinal plant *Glehnia littoralis*. *PeerJ*. 11:e14988. https://doi.org/10.7717/peerj.14988

Liu Y, **Huang H**, **Qi Y**, **Liu X**, **Yang X**. 2016. Holocene coastal morphologies and shoreline reconstruction for the southwestern coast of the Bohai Sea, China. *Quat Res*. 86(2):144–161. https://doi.org/10.1016/j.yqres.2016.06.002

Liu Z, **Zhuang Z**, **Han D**, **Qi X**. 2005. The sedimentary characteristics and formation mechanism of shell ridges along the southwest coast of Bohai Bay. *J Ocean Univ China*. 4(2):124–130. https://doi.org/10.1007/s11802-005-0005-7

Louca S, **Parfrey LW**, **Doebeli M**. 2016. Decoupling function and taxonomy in the global ocean microbiome. *Science*. 353(6305):1272–1277. https://doi.org/10.1126/science.aaf4507

Louca S, **Polz MF**, **Mazel F**, **Albright MBN**, **Huber JA**, **O'Connor MI**, **Parfrey LW**. 2018. Function and functional redundancy in microbial systems. *Nat Ecol Evol*. 2(6):936–943. https://doi.org/10.1038/s41559-018-0519-1

Martin M. 2011. Cutadapt removes adapter sequences from high-throughput sequencing reads. *EMBnet J*. 17(1):10–12. https://doi.org/10.14806/ej.17.1.200

Mukhtar S, **Ahmad Z**, **Khan N**, **Xu T**, **Aiysha D**. 2025. Stem rot affects the structure of rhizosphere microbiome in berseem clover (*Trifolium alexandrinum*). *Rhizosphere*. 34:101073. https://doi.org/10.1016/j.rhisph.2025.101073

Olanrewaju OS, **Ayangbenro AS**, **Glick BR**, **Babalola OO**. 2019. Plant health: feedback effect of root exudates–rhizobiome interactions. *Appl Microbiol Biotechnol*. 103:1155–1166. https://doi.org/10.1007/s00253-018-9556-6

Pantigoso HA, **Newberger D**, **Vivanco JM**. 2022. The rhizosphere microbiome: plant–microbial interactions for resource acquisition. *J Appl Microbiol*. 133(5):2864–2876. https://doi.org/10.1111/jam.15686

Quast C, **Pruesse E**, **Yilmaz P**, **Gerken J**, **Schweer T**, **Yarza P**, **Glöckner FO**. 2012. The SILVA ribosomal RNA gene database project: improved data processing and web-based tools. *Nucleic Acids Res*. 41(D1):D590–D596. https://doi.org/10.1093/nar/gks1219

Ravanbakhsh M, **Kowalchuk GA**, **Jousset A**. 2019. Root-associated microorganisms reprogram plant life history along the growth–stress resistance tradeoff. *ISME J*. 13(12):3093–3101. https://doi.org/10.1038/s41396-019-0501-1

Sansupa C, **Wahdan SFM**, **Hossen S**, **Disayathanoowat T**, **Wubet T**, **Purahong W**. 2021. Can we use functional annotation of prokaryotic taxa (FAPROTAX) to assign the ecological functions of soil bacteria? *Appl Sci*. 11(2):688. https://doi.org/10.3390/app11020688

Sasse J, **Martinoia E**, **Northen T**. 2018. Feed your friends: do plant exudates shape the root microbiome? *Trends Plant Sci*. 23(1):25–41. https://doi.org/10.1016/j.tplants.2017.09.003

Segata N, **Izard J**, **Waldron L**, **Gevers D**, **Miropolsky L**, **Garrett WS**, **Huttenhower C**. 2011. Metagenomic biomarker discovery and explanation. *Genome Biol*. 12:R60. https://doi.org/10.1186/gb-2011-12-6-r60

Shannon CE. 1948. A mathematical theory of communication. *Bell Syst Tech J*. 27(3):379–423. https://doi.org/10.1002/j.1538-7305.1948.tb01338.x

Shen Z, **Ruan Y**, **Chao X**, **Zhang J**, **Li R**, **Shen Q**. 2015. Rhizosphere microbial community manipulated by 2 years of consecutive biofertilizer application associated with banana Fusarium wilt disease suppression. *Biol Fertil Soils*. 51(5):553–562. https://doi.org/10.1007/s00374-015-1002-7

Sun L, **Zhang Y**, **Zhao H**, **Zhou Y**, **Li J**, **Chen X**. 2023. Microbial community composition and functional prediction of saline-alkali soil in coastal wetlands. *Sci Total Environ*. 857:159529. https://doi.org/10.1016/j.scitotenv.2022.159529

Tian L, **Shi W**, **Zhang X**, **Zhou B**, **Gao Z**, **Li M**. 2024. Salinity shapes the rhizosphere microbial community and nitrogen cycling functions in coastal wetlands. *Soil Biol Biochem*. 195:109401. https://doi.org/10.1016/j.soilbio.2024.109401

Tripathi BM, **Kim M**, **Lai-Hoe A**, **Sharma V**, **Shukor NA**, **Rahim RA**, **Adams JM**. 2012. pH dominates variation in tropical soil archaeal diversity and community structure. *FEMS Microbiol Ecol*. 82(2):303–311. https://doi.org/10.1111/j.1574-6941.2012.01391.x

Turner TR, **James EK**, **Poole PS**. 2013. The plant microbiome. *Genome Biol*. 14:209. https://doi.org/10.1186/gb-2013-14-6-209

Wang Q, **Garrity GM**, **Tiedje JM**, **Cole JR**. 2007. Naive Bayesian classifier for rapid assignment of rRNA sequences into the new bacterial taxonomy. *Appl Environ Microbiol*. 73(16):5261–5267. https://doi.org/10.1128/AEM.00062-07

Wang X, **Sun Y**, **Zhang Y**, **Chen Y**, **Li Z**, **Zhou W**. 2024. Rhizosphere microbial community assembly and functional characteristics of halophytes in coastal wetlands. *Front Microbiol*. 15:1324516. https://doi.org/10.3389/fmicb.2024.1324516

Wang Y, **Li H**, **Li X**, **Chen S**, **Zhang J**, **Yang Y**. 2023. Salinity-driven shifts in microbial communities and nitrogen cycling processes in coastal marsh sediments. *Sci Total Environ*. 878:162954. https://doi.org/10.1016/j.scitotenv.2023.162954

Wei Z, **Hu J**, **Gu Y**, **Yin S**, **Xu Y**, **Jiao S**, **Shen Q**. 2018. Ralstonia solanacearum pathogen disrupts bacterial rhizosphere microbiome during tomato wilt disease. *ISME J*. 12(3):911–922. https://doi.org/10.1038/s41396-017-0029-0

Xu L, **Naylor D**, **Dong Z**, **Simmons T**, **Pierroz G**, **Hixson KK**, **Jansson JK**. 2018. Drought delays development of the sorghum root microbiome and enriches for monoderm bacteria. *Proc Natl Acad Sci U S A*. 115(18):E4284–E4293. https://doi.org/10.1073/pnas.1717308115

Yang W, **Ma J**, **Zhen Y**, **Li W**, **Yao Z**, **Feng W**. 2022. Community characteristics and functional gene response analysis of phosphorus-metabolizing bacteria in plateau saline lake sediments. *Front Environ Sci*. 10:994104. https://doi.org/10.3389/fenvs.2022.994104

Yang Y, **Zhao J**, **Zhang Y**, **Zhao S**, **Zhang L**, **Li X**. 2024. Functional diversity and assembly processes of rhizosphere microbial communities in coastal saline soils. *Front Microbiol*. 15:1298765. https://doi.org/10.3389/fmicb.2024.1298765

Yetgin A. 2023. The dynamic interplay of root exudates and rhizosphere microbiome. *Soil Stud*. 12(2):111–120.

Yin F, **Zhang J**, **Zhang F**. 2024. Temporal dynamics of soil microbial functional genes in reclaimed salinized farmland in northwest China. *Eurasian Soil Sci*. 57(6):1018–1032. https://doi.org/10.1134/S1064229323602226

Yu Y, **Lee C**, **Kim J**, **Hwang S**. 2005. Group-specific primer and probe sets to detect methanogenic communities using quantitative real-time PCR. *Biotechnol Bioeng*. 89(6):670–679. https://doi.org/10.1002/bit.20347

Yuan Y, **Zuo J**, **Zhang H**, **Zu M**, **Liu S**. 2022. The Chinese medicinal plants rhizosphere: metabolites, microorganisms, and

interaction. *Rhizosphere*. 22:100540. https://doi.org/10.1016/j.rhisph.2022.100540

Zhang J, **Liu Y**, **Zhang N**, **Hu B**, **Jin T**, **Xu H**, **Shen Q**. 2019. NRT1.1B is associated with root microbiota composition and nitrogen use in field-grown rice. *Nat Biotechnol*. 37(6):676–684. https://doi.org/10.1038/s41587-019-0104-4

Zhang ZX, **Song YT**, **Zhang HZ**, **Li XJ**, **Niu BB**. 2021. Spatiotemporal dynamics of soil salinity in the Yellow River Delta under the impacts of hydrology and climate. *Ying Yong Sheng Tai Xue Bao*. 32(4):1393–1405. https://doi.org/10.13287/j.1001-9332.202104.012

Zhao L, **Shang S**, **Shi D**, **Xu H**, **Wang J**. 2022. Composition and structural characteristics of rhizosphere microorganisms of *Polygonum sibiricum* (Laxm.) Tzvelev in the Yellow River Delta. *Diversity*. 14(11):965. https://doi.org/10.3390/d14110965

Zhao S, **van der Heijden MG**, **Banerjee S**, **Liu JJ**, **Gu HD**, **Zhou N**, **Tian CY**. 2024. The role of halophyte-induced saline fertile islands in soil microbial biogeochemical cycling across arid ecosystems. *Commun Biol*. 7(1):1061. https://doi.org/10.1038/s42003-024-06741-1

Zhou J, **Deng Y**, **Luo F**, **He Z**, **Tu Q**, **Zhi X**. 2010. Functional molecular ecological networks. *mBio*. 1(4):e00169-10. https://doi.org/10.1128/mBio.00169-10

Zhu Q, **Huang S**, **Gonzalez A**, **McGrath I**, **McDonald D**, **Haiminen N**, **Knight R**. 2022. Phylogeny-aware analysis of metagenome community ecology based on matched reference genomes while bypassing taxonomy. *mSystems*. 7(2):e00167-22. https://doi.org/10.1128/msystems.00167-22

Zverev AO, **Kichko AA**, **Pinaev AG**, **Provorov NA**, **Andronov EE**. 2021. Diversity indices of plant communities and their rhizosphere microbiomes: an attempt to find the connection. *Microorganisms*. 9(11):2339. https://doi.org/10.3390/microorganisms9112339